

Flat bands in fractal-like geometry

Biplab Pal* and Kush Saha†

Max Planck Institute for the Physics of Complex Systems, Nöthnitzer Str. 38, 01187 Dresden, Germany

We report the presence of multiple flat bands in a class of two-dimensional (2D) lattices formed by Sierpinski gasket (SPG) fractal geometries as the basic unit cells. Solving the tight-binding Hamiltonian for such lattices with different generations of a SPG network, we find multiple degenerate and non-degenerate *completely flat* bands, depending on the configuration of parameters of the Hamiltonian. Moreover, we establish a generic formula to determine the number of such bands as a function of generation index, ℓ of the fractal geometry. We show that the flat bands and their neighboring dispersive bands have remarkable features, the most interesting one being the spin-1 conical-type spectrum at the band center without any staggered magnetic flux, in contrast to the Kagome lattice. We furthermore investigate the effect of magnetic flux in these lattice settings and show that different combinations of fluxes through such fractal unit cells lead to richer spectrum with a single isolated flat band or gapless electron- or hole-like flat bands. Finally, we discuss a possible experimental setup to engineer such fractal flat band network using single-mode laser-induced photonic waveguides.

I. INTRODUCTION

Over the course of last few years, the study of flat bands (FBs) in translationally invariant lattice systems has been one of the emergent fields of research in condensed matter physics [1–15]. This is in part because such bands can serve as a good platform for studying strongly correlated phenomena due to exponentially large number of degeneracy, and in part because they can host many interesting phenomena such as unconventional inverse Anderson transition [1, 2], multifractality at weak disorder [3, 4], Hall ferromagnetism [16–18], etc. In addition, there are rising interests in finding out lattice models that can host FBs with non-trivial topology. This is because such non-trivial FBs may allow one to investigate lattice version of fractional topological phenomena [19–21]. Above all, the recent experimental observations of FBs in various photonic lattices [22–29], optical lattices [30–32], and exciton-polariton condensates [33] have triggered a great deal of interest in generating new FB networks and understanding their usage in different lattice geometry.

The appearance of FBs in translationally invariant tight-binding models is often attributed to the destructive interference of electrons hopping nonlocally, giving rise to compact localized single-particle eigenstates (CLS) with finite amplitudes over a finite number of lattice sites beyond which the wave function amplitudes decay to zero [10, 13, 14]. Specifically, the electrons in these FB states do not hop to the neighboring lattice sites, leading to strongly localized states with an infinite effective band mass. FBs with non-trivial topology can be obtained in lattice models by fine-tuning the short-range hopping strengths between different lattice sites or by incorporating some artificial phase factors to the

hopping parameters [19, 21]. Recently, it has also been shown that FBs with chiral symmetry can be realized in bipartite lattices by creating imbalance in number of sites between the two sublattices [15].

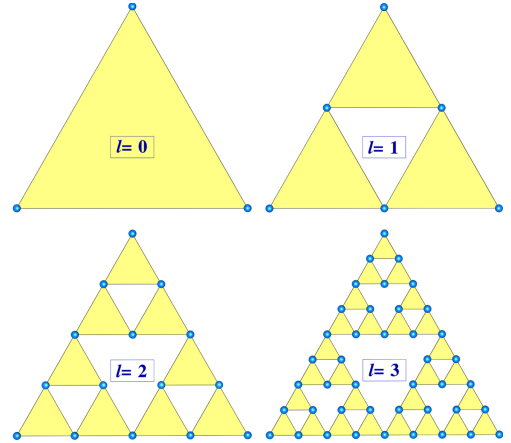


FIG. 1: Schematic view of different generations (ℓ) of a Sierpinski gasket (SPG) fractal network, which are repeated periodically over a two-dimensional plane to form 2D lattices with fractal unit cell.

While there are extensive studies on FBs for regular periodic lattices such as Lieb [4, 22, 23, 26, 30, 32], Kagome [28, 33–37], hexagonal [5, 38], diamond [9, 13, 24, 25], cross-switch [10–12], etc., the possibility of having FBs with various interesting band features in two-dimensional (2D) lattices with fractal unit cells has not been reported yet. We show that the 2D lattices built with different generations of a Sierpinski gasket (SPG) fractal network [39] (see Fig. 1) as the unit cells can host multiple degenerate and non-degenerate FBs, depending on the intra and inter-cell hopping strengths. These FBs and their nearest dispersive bands have distinct features such as “isolated” degenerate FBs, conical “Dirac-like” bands together with a single flat band at the center of the energy spectrum, and many more. These band fea-

*Electronic address: biplabpal@pks.mpg.de

†Electronic address: kush@pks.mpg.de

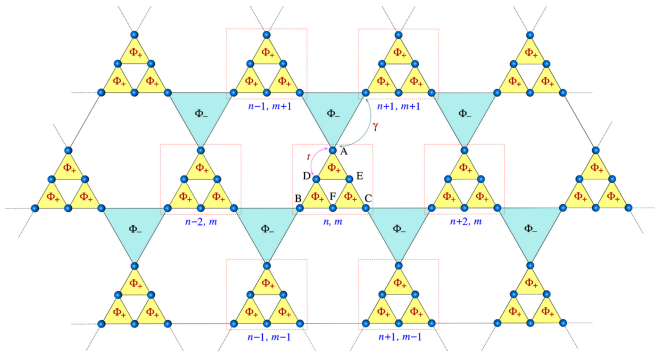


FIG. 2: Schematic diagram of a two-dimensional lattice structure where the building blocks (unit cells) are first generation ($\ell = 1$) SPG fractal geometry. Each of the “up” triangular plaquettes (light yellow shaded) within the SPG unit cell are threaded by an external magnetic flux Φ_+ , whereas the “down” triangles (light blue shaded) connecting nearest unit cells carry a flux Φ_- . Each cell has been marked by the red dotted box. The intra-cell hopping parameter is denoted by t and the inter-cell hopping parameter is labeled by γ .

tures differ significantly from the Kagome (*i. e.*, $\ell = 0$ generation of the SPG) or Lieb lattice. We furthermore show that the number of such FBs increases with the increase of fractality *i. e.*, the generation index ℓ of the fractal unit cells. In fact, we find a generic formula to determine the number of FBs as a function of ℓ .

We also investigate the effect of an external magnetic field in this lattice model and show that the different combinations of magnetic fluxes piercing through the “up” and “down” triangles of the lattice structure (see Fig. 2) give rise to spectrum with notable features. They are classified into three types: (I) a *single* isolated flat band at the middle of the band spectrum, separating electron-like and hole-like dispersive bands, (II) a *single gapless* hole-like or electron-like flat band, and (III) two *gapless* parallel electron-hole flat bands separated by their respective electron-like and hole-like dispersive bands. These parallel FBs turn out to be robust under unequal hopping strengths. We note that these flat bands at different energies in the absence of time-reversal symmetry can be leveraged to understand several physical phenomena such as quantum Hall phenomena at fractional filling, chiral spin liquid physics, topological transitions, etc [37].

The rest of the paper is organized as follows. In Sec. II, we introduce and discuss the tight-binding Hamiltonian of spinless particles moving in a two-dimensional lattice formed by fractal unit cells. This is followed by Sec. III, where we discuss different features of FBs and their neighboring dispersive bands, in the absence of any external magnetic flux. Moreover, we demonstrate local density of states and show distribution of wavefunction amplitudes at different lattice sites. In Sec. IV, we present the results for staggered and non-staggered magnetic flux. In Sec. V, we discuss the scope of possible experimental realization of our model, using photonic waveguide lattice structure. Finally, we conclude with a

discussion on the usefulness of the proposed lattice model and possible future directions in Sec. VI.

II. THE MODEL

We propose a class of two-dimensional lattice models where segment of fractal geometries act as a constituent unit cell of the lattice structure. Fig. 2 illustrates such a lattice structure where first generation ($\ell = 1$) of a SPG fractal plays the role of the unit cell. Similar structures can be constructed using other higher generations of the SPG fractal geometry acting as the unit cell of the lattice. For simplicity, we focus on the $\ell = 1$ generation of SPG with six atoms per unit cell. With this, the tight-binding Hamiltonian can be written in Wannier basis as,

$$H = \sum_{n,m} \left[\sum_{j=A}^F \epsilon_j c_{n,m,j}^\dagger c_{n,m,j} + \left(t c_{n,m,A}^\dagger c_{n,m,D} + t c_{n,m,A}^\dagger c_{n,m,E} + t c_{n,m,B}^\dagger c_{n,m,D} + t c_{n,m,B}^\dagger c_{n,m,F} + t c_{n,m,C}^\dagger c_{n,m,F} + t c_{n,m,C}^\dagger c_{n,m,E} + t c_{n,m,D}^\dagger c_{n,m,E} + t c_{n,m,E}^\dagger c_{n,m,F} + t c_{n,m,F}^\dagger c_{n,m,D} + \gamma c_{n,m,A}^\dagger c_{n+1,m+1,B} + \gamma c_{n,m,A}^\dagger c_{n-1,m+1,C} + \gamma c_{n,m,C}^\dagger c_{n+2,m,B} + h.c. \right) \right], \quad (1)$$

where (n, m) stands for the cell index, and the letters A, B, C, D, E, F identify different atomic sites within a cell as depicted in Fig. 2. $c_{n,m,j}^\dagger$ ($c_{n,m,j}$) creates (annihilates) an electron in the (n, m) -th cell for atomic site j , ϵ_j is the on-site potential for a j -type of atomic site, t is the intra-cell hopping amplitude, and γ denotes the inter-cell hopping amplitude.

In $\mathbf{k} \equiv (k_x, k_y)$ -space, Eq. (1) can be recast as,

$$H = \sum_{\mathbf{k}} \psi_{\mathbf{k}}^\dagger \mathcal{H}(\mathbf{k}) \psi_{\mathbf{k}}, \quad (2)$$

where $\psi_{\mathbf{k}}^\dagger \equiv (c_{\mathbf{k},A}^\dagger \ c_{\mathbf{k},B}^\dagger \ c_{\mathbf{k},C}^\dagger \ c_{\mathbf{k},D}^\dagger \ c_{\mathbf{k},E}^\dagger \ c_{\mathbf{k},F}^\dagger)$, and $\mathcal{H}(\mathbf{k})$ is given by,

$$\mathcal{H}(\mathbf{k}) = \begin{pmatrix} \mathcal{M}(\mathbf{k}) & \mathcal{T} \\ \mathcal{T}^\dagger & \mathcal{G} \end{pmatrix}, \quad (3)$$

where $\mathcal{M}(\mathbf{k})$ is a square matrix of dimension three for all ℓ , and is given by,

$$\mathcal{M}(\mathbf{k}) = \begin{pmatrix} \epsilon_A & \gamma e^{i(k_x+k_y)} & \gamma e^{-i(k_x-k_y)} \\ \gamma e^{-i(k_x+k_y)} & \epsilon_B & \gamma e^{-2ik_x} \\ \gamma e^{i(k_x-k_y)} & \gamma e^{2ik_x} & \epsilon_C \end{pmatrix}. \quad (4)$$

Note that the off-diagonal matrix elements of $\mathcal{M}(\mathbf{k})$ connect the nearest unit cells. In contrast, the matrix elements of \mathcal{G} and \mathcal{T} represent hopping within the same cell and hence independent of the momentum \mathbf{k} . For $\ell = 1$, they can be expressed in appropriate basis as,

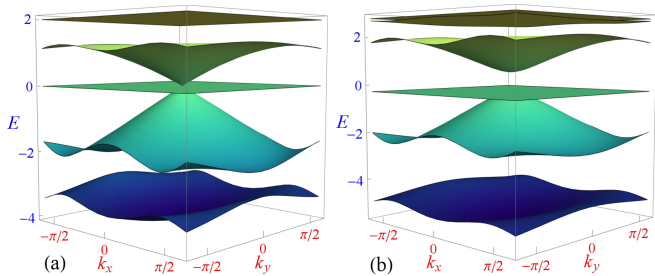


FIG. 3: Energy dispersions for $\ell = 1$ generation SPG fractal network acting as the unit cell of the 2D lattice structure in Fig. 2 with $\Phi_{\pm} = 0$. The left panel corresponds to $t/\gamma = 1$ (with $t = -1$ and $\gamma = -1$), while the right panel is for $t/\gamma \neq 1$ (with $t = -1.5$ and $\gamma = -1$).

$$\mathcal{G} = \begin{pmatrix} \epsilon_D & t & t \\ t & \epsilon_E & t \\ t & t & \epsilon_F \end{pmatrix}, \quad \mathcal{T} = \begin{pmatrix} t & t & 0 \\ t & 0 & t \\ 0 & t & t \end{pmatrix}. \quad (5)$$

For generic ℓ , \mathcal{G} is a square matrix of dimension $(\mathcal{N}_{\ell} - 3)$, while the dimension of \mathcal{T} is found to be $(\mathcal{N}_{\ell} - 3) \times 3$, where \mathcal{N}_{ℓ} is the number of atoms per unit cell. It is worth mentioning that Eq. (3) is written in a basis which does not incorporate lattice symmetry (e.g., triangular symmetry). However, it can be shown that Hamiltonian in accordance with the lattice symmetry gives rise to similar spectrum as shown here.

To incorporate the effect of generic magnetic flux, we consider a flux Φ_+ per “up” triangular plaquette (light yellow shaded) in the SPG unit cell as shown in Fig. 2. Then the flux penetrating through the middle down triangle of the same unit cell turns out to be $-\Phi_+$. We further consider the flux penetrating through the “down” triangles (light blue shaded) connecting the two nearest SPG unit cells to be Φ_- as shown in Fig. 2. This fixes the flux through the hexagon to be equal to $-(2\Phi_+ + \Phi_-)$, when Φ_{\pm} are considered *anticlockwise*. With this construction, the matrix elements t 's of \mathcal{H} in Eq. (3) pick up a prefactor $e^{\pm i\Phi_+/3}$, while the γ 's pick up $e^{\pm i\Phi_-/3}$, where the sign of the phases is to be considered in accordance with the direction of the hopping.

III. FLAT BANDS IN ZERO FLUX

To analyze the energy spectrum for $\Phi_{\pm} = 0$, we diagonalize Eq. (3) and obtain six bands for $\ell = 1$ generation SPG unit cell, containing multiple *completely flat* and dispersive bands. Depending on the relative strengths between the intra- and inter-cell hopping, these flat bands may be degenerate or non-degenerate. Moreover, the number of flat bands increases with the generation index, ℓ .

Equal intra and inter-cell hopping — For $t = \gamma$ and $\ell = 1$, the flat bands energies are

$$E_{\text{FB}} = -2t, -2t, 0. \quad (6)$$

Fig. 3(a) shows that the doubly degenerate flat bands occur at the maximum of the spectrum and are *isolated* from rest of the other bands. This is in contrast to the commonly known “frustrated hopping” model [35] such as Kagome, where non-degenerate isolated flat-band can be obtained only in the presence of magnetic flux [36]. The non-degenerate flat band at $E = 0$ touches “Dirac-point” formed by two electron-hole dispersive bands at $\mathbf{k} = 0$, and they all together form a spin-1 conical-type spectrum. These three bands at the center of the spectrum resembles with the spectrum of Kagome lattice with staggered flux [36] or Lieb lattice with zero flux [22, 23, 26, 30, 32]. Note that, the $\mathbf{k} = 0$ Dirac point can be regarded as a special point where particle can have both zero effective mass (Dirac fermions) and infinite effective mass (FB state). Note also, the presence of this single Dirac point in the spectrum seems to violate fermion-doubling theorem. However, this is in consistent with the fact that fermion-doubling theorem can be avoided by introducing a flat band in the system [40].

For $\ell = 2$ generation, the flat bands appear at the energies

$$E_{\text{FB}} = -2t, -2t, -2t, -2t, -2t, -t, t f_{\alpha}(t), \quad (7)$$

where α runs from 1 to 3, and $f(t)$ is some complicated function of t . Thus, we have five-fold degenerate FBs at $E = -2t$, and rest are non-degenerate with two electron-like and two hole-like FBs, as evident from Fig. 4(a). We have exclusively checked energy spectrum for higher generations (see Fig. 4(c)) and found that the number of FBs increases with the generation index ℓ . In fact, we find a generalized formula to determine the number of FBs in a $(\ell + 1)$ -th generation fractal. This is given by,

$$\mathcal{F}_{\ell+1} = \mathcal{N}_{\ell+1} - \mathcal{D}_{\ell+1} \quad \text{for } \ell \geq 0, \quad (8)$$

where $\mathcal{D}_{\ell+1}$ is the total number of dispersive bands (DBs) in a $(\ell + 1)$ -th generation fractal, and is given by $\mathcal{D}_{\ell+1} = 2\mathcal{D}_{\ell}$ for $\ell \geq 1$ with $\mathcal{D}_1 = 3$. $\mathcal{N}_{\ell+1}$ is the total number of lattice sites in a $(\ell + 1)$ -th generation fractal unit cell, and is given by $\mathcal{N}_{\ell+1} = 3\mathcal{N}_{\ell} - 3$ for $\ell \geq 1$ with $\mathcal{N}_1 = 6$.

Unequal intra and inter-cell hopping — In contrast to $t = \gamma$, the unequal intra and inter-cell hopping, *i. e.*, $t \neq \gamma$ reduces the number of flat bands and the degeneracy as well. For $\ell = 1$, we obtain two FBs with energies (see Fig. 3(b))

$$E_{\text{FB}} = \frac{1}{2} \left(-\gamma - t + \sqrt{(\gamma - t)^2 + 4t^2} \right) \\ E_{\text{FB}} = -\frac{1}{2} \left(\gamma + t + \sqrt{(\gamma - t)^2 + 4t^2} \right), \quad (9)$$

whereas for $\ell = 2$ generation, we obtain eight FBs (see Fig. 4(b)) at energies

$$E_{\text{FB}} = -2t, -2t, -2t, -t, f'_{\alpha}(t, \gamma), \quad (10)$$

where α runs from 1 to 4, and $f'(t, \gamma)$ is some complicated function of t and γ . Clearly, the number of FBs

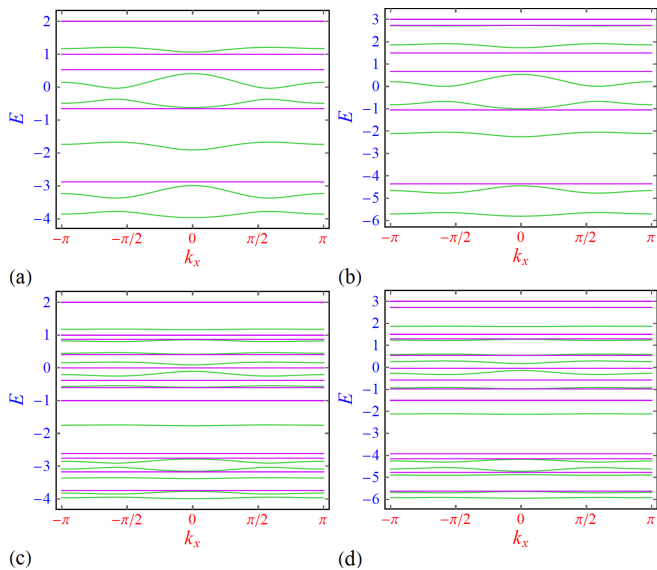


FIG. 4: E - k diagram for (a-b) $\ell = 2$, and (c-d) $\ell = 3$ generation of SPG fractal unit cell. The *completely* flat bands are marked by the violet color flat lines, whereas dispersive or nearly flat bands are marked by green color. For the left panel the ratio between intra-cell and inter-cell hopping is taken to be $t/\gamma = 1$, whereas for the right panel it is $t/\gamma = 1.5$.

and the degeneracy are reduced. Also, unequal value of the hopping parameters lifts the degeneracy at the Dirac-point in conical-like spectrum since a finite gap appears between the FB and hole-like Dirac band (see Fig. 3(b)). However, the degeneracy between the FB and its neighboring electron-like dispersive band is retained at $\mathbf{k} = 0$. This band touching turns out to be linear unlike the case in Kagome lattice. Note that, this band feature is reminiscent to the spectrum of artificial ice due to point-like dipole with fine-tuned external offset parameter related to sublattice [41]. Thus, for finite filling our lattice model may reveal interesting spin-ice physics. Investigating higher generations (Fig. 4) as before, we find a generalized formula for determining FBs for $t \neq \gamma$ as,

$$\mathcal{F}_{\ell+1} = \mathcal{N}_{\ell+1} - \mathcal{D}_{\ell+1} \quad \text{for } \ell \geq 0, \quad (11)$$

where $\mathcal{D}_{\ell+1} = 2\mathcal{D}_{\ell} - 1$ for $\ell \geq 1$ with $\mathcal{D}_1 = 4$, and $\mathcal{N}_{\ell+1}$ is same as before.

As discussed, the completely flat band states are generated by highly localized eigenstates. To corroborate this fact, we compute average density of states (ADOS) corresponding to the cases presented in Fig. 3(a) and 3(b). Using standard Green's function formalism, the ADOS is defined as,

$$\rho(E) = -\frac{1}{N\pi} \text{Im} [\text{Tr } \mathbf{G}(E)], \quad (12)$$

where $\mathbf{G}(E) = [(E + i\eta)\mathbf{I} - \mathbf{H}]^{-1}$ with η being a small imaginary part added to the energy E , N is total number of sites in the system, 'Im' is the imaginary part, and 'Tr' denotes the trace of the Green's function \mathbf{G} .

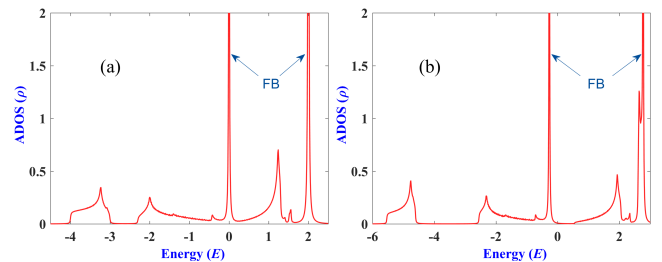


FIG. 5: Average density of states (ADOS) for $\ell = 1$ generation SPG unit cells repeated in X - Y direction to form a 2D lattice structure with size $L = (40 \times 40)$ as shown in Fig. 2. The left panel corresponds to $t/\gamma = 1$ (with $t = -1$ and $\gamma = -1$), while the right panel is for $t/\gamma \neq 1$ (with $t = -1.5$ and $\gamma = -1$). The states corresponding to the flat bands (FB) are indicated by the arrowheads.

Together with Eq. (12) and (1), we compute the ADOS for $\ell = 1$ generation SPG structure with system size $L = 40$. Fig. 5(a) and 5(b) show very sharp localized states in the ADOS for field free case. The appearance of such localized states can be traced back to the presence of flat band states in the energy spectrum as shown in Fig. 3(a) and 3(b). We note that the ADOS for the cases with the magnetic field shows similar highly peaked localized states at corresponding flat band energies.

We next turn to distribution of wave function amplitudes at different lattice sites, which can be easily evaluated using the Schrödinger equation of the form,

$$(E - \epsilon_i) \psi_i = \sum_j \tau_{ij} \psi_j, \quad (13)$$

where ϵ_i is the on-site potential at i -th site, τ_{ij} is the hopping amplitude between neighboring sites, and ψ_i is the wave function amplitude at i -th site. Fig. 6(a) and 6(b)

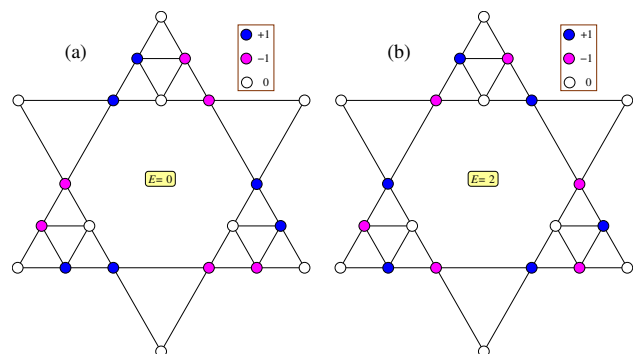


FIG. 6: Distribution of wave function amplitudes at different lattice sites corresponding to highly localized FB states with energies (a) $E = 0$ and (b) $E = 2$ as shown in Fig. 5(a). The on-site potential for all the sites is set to zero, and the hopping parameters are $t = -1$ and $\gamma = -1$ respectively. The values of the wave function amplitudes on different lattice sites are +1 (blue/dark filled circles), -1 (magenta/light filled circles), and 0 (empty circles).

illustrates the wave function amplitude distribution cor-

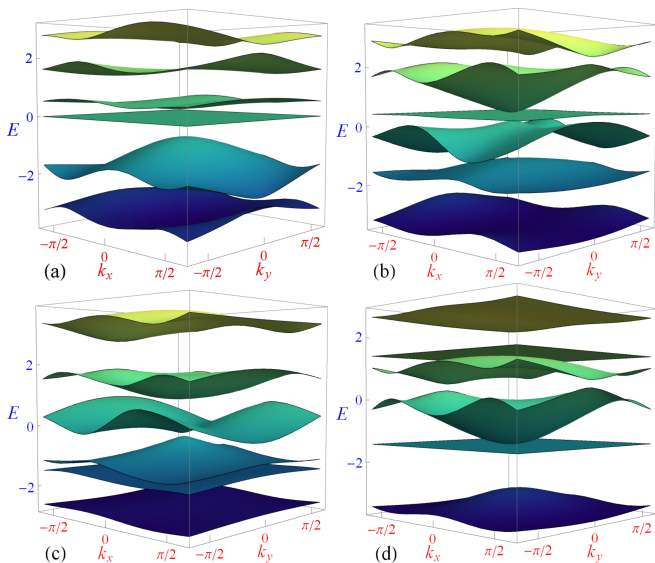


FIG. 7: Energy dispersions in presence of the staggered magnetic fluxes Φ_{\pm} for $\ell = 1$ generation SPG fractal geometry. Different panels correspond to different combinations of fluxes Φ_{+} and Φ_{-} , *viz.*, (a) $\Phi_{+} = \Phi_{-} = \pi/3$, (b) $\Phi_{+} = \pi/3$ and $\Phi_{-} = -\pi$, (c) $\Phi_{+} = -\pi$ and $\Phi_{-} = \pi/3$, and (d) $\Phi_{+} = 2\pi$ and $\Phi_{-} = \pi$. We have used $t/\gamma = 1$.

responding to the FB states with energies $E = 0$ and $E = 2$ as shown in Fig. 5(a). Evidently, the wave function corresponding to the FB states are localized over a finite number of lattice sites with non-zero amplitudes (marked by filled circles), and beyond those sites the amplitudes of the wavefunction turns out to be zero (marked by empty circles). Using the same procedure, one can also figure out similar kind of wave function amplitude distribution pattern corresponding to the FB energies shown in Fig. 5(b).

IV. EFFECT OF MAGNETIC FLUX ON FLAT BANDS

The objective of this section is to investigate the fate of flat bands in the presence of staggered magnetic flux Φ_{\pm} (measured in units of the fundamental flux quantum $\Phi_0 = h/e$) piercing through the triangular plaquettes in the fractal lattice geometry as shown in Fig. 2. It turns out that generic magnetic flux destroys FBs, leading to gapped dispersive bands. This destruction is independent of the relative strength between the hopping parameters t and γ . However, for special values of Φ_{\pm} , flat bands reappear and can be classified into three types.

For $t = \gamma$ and $\Phi_{+} = \Phi_{-} = \pi/3$, we obtain a single isolated flat band at $E_{\text{FB}} = 0$, separating three hole-like and two electron-like dispersive bands, as shown in Fig. 7(a). The two electron-like dispersive bands resemble the spectrum of gapped graphene in the absence of time-reversal symmetry [42]. Since this isolated flat band is protected by the gap, the degenerate states can be used to form

correlated states when interactions are added. Note that, the isolated FB acquires a small curvature as intra-cell and inter-cell hopping differs from each other.

In contrast, for $\Phi_{+} = \pm\pi/3$ and $\Phi_{-} = \mp\pi$, we obtain a single gapless flat band with energy $E_{\text{FB}} > 0$. Moreover, this FB touches its nearest dispersive band at a single point in the Brillouin zone (see Fig. 7(b)), and the band touching turns out to be linear similar to the band touching discussed in the preceding section. However, the band touching can be removed by unequal intra-cell and inter-cell hopping, keeping the FB *nearly* flat. For a reverse combination of Φ_{+} and Φ_{-} , we do not see any gapless flat bands, rather two nearly FBs appear at the end of the band spectrum as shown in Fig. 7(c).

At $\Phi_{+} = \Phi_{-} = \pm\pi$, the spectrum is particle-hole conjugate of the case at $\Phi_{\pm} = 0$. With this combination of fluxes, the total flux through the individual unit cell and the down triangle connecting nearest unit cells turns out to be $(2\Phi_{+} - \Phi_{-}) = \pm 3\pi$ or $\pm\pi$. The first condition is exactly similar to the condition for staggered fluxes in “up” and “down” triangles of Kagome lattice [36] as a manifestation of time-reversal symmetry, while the latter is typical time-reversal symmetric non-staggered case of $n\pi$ flux through each plaquette, where n is integer.

In addition to the above combinations of Φ_{\pm} 's, we obtain a particular combination of fluxes such that $(\Phi_{+} + \Phi_{-}) = \pi$ (with $\Phi_{+} = 0$ (or π) and $\Phi_{-} = \pi$ (or 0)), or 3π (with $\Phi_{+} = 2\pi$ (or π) and $\Phi_{-} = \pi$ (or 2π)), for which two flat bands are separated by two dispersive bands. Fig. 7(d) illustrates this specific case, where we see both the electron-like and hole-like flat bands touch their nearest dispersive bands at a single point in the first BZ. Interestingly, the nature of band touching is quite different for these two FBs. While one FB touches quadratically to its nearest dispersive band, the other one touches the dispersive band linearly. Moreover, both of these band touching are protected from any perturbation in the Hamiltonian. Notice that, in this particular case, there exists an isolated nearly flat band at the maximum or minimum of the spectrum.

It is worth pointing out that there are some other combinations of fluxes for which a flat band and its nearest dispersive band overlap, which we do not elaborate here in order to not deviate from the main interesting features discussed in the preceding sections. We would also like to mention that similar distinct band features can be obtained for higher generation fractal structures in presence of the external staggered flux.

Before ending this section, we briefly discuss the real space energy spectrum of a *single* unit cell of the SPG fractal structure in the thermodynamic limit as a function of magnetic flux. We consider each smallest “up” triangular plaquettes in the unit cell carries flux Φ_{+} . Then following Ref. [43], we compute the energy eigenvalues as a function of Φ_{+} . Fig. 8 illustrates the formation of bands and gaps in the spectrum. Clearly, the thinning of bands at $\Phi_{+} = 0$ and its conjugate case, *i. e.*, $\Phi_{+} = \pi$ is attributed to the presence of FBs.

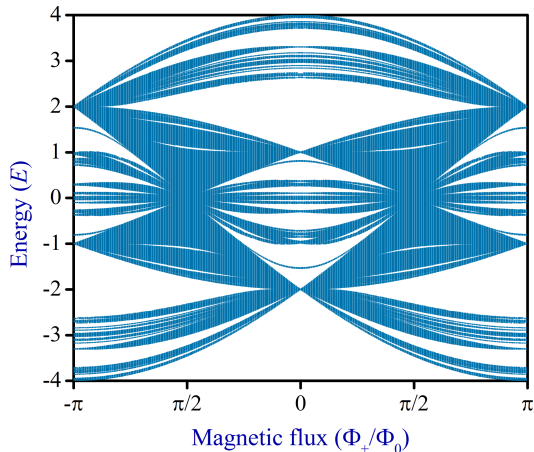


FIG. 8: Energy eigenvalue spectrum of a SPG fractal geometry in the thermodynamic limit as a function of the magnetic flux Φ_+ (measured in units of the fundamental flux quantum $\Phi_0 = h/e$). We have set the on-site potentials at all sites to be equal to zero and the hopping parameter t is taken equal to 1.

V. POSSIBLE EXPERIMENTAL REALIZATION

Finally, we discuss the scope for possible experimental realization of our proposed complex lattice structure and related phenomena. In the spirit of recent experiments by Mukherjee *et al.* [23, 24] and also by others [22, 27, 28], photonic lattices formed by laser-induced single-mode waveguides can be used to study different FB properties discussed here, in the absence of undesired excitations such as phonons. In such photonic structure, the atomic sites in our proposed 2D fractal lattice geometry can be replaced by single-mode optical waveguides, which can be controlled by femtosecond laser-writing technique as well as the optical induction technique. This may allow one for direct observations of diffractionless FB states. A schematic diagram of the possible corresponding photonic waveguide structure of our proposed model (for $\ell = 1$ generation SPG geometry acting as the unit cell of the lattice) is illustrated in Fig. 9. The intra- and inter-cell hopping parameters can be controlled by the refractive index of the lattice structure. Moreover, by modulating longitudinal propagation constants [25, 44] of the waveguides, a synthetic gauge field can be generated to study the effect of magnetic the flux in our proposed lattice geometry. In addition to the photonic lattices, the unprecedented controllability of cold atoms in optical lattices may help to engineer such artificial complex structures in experiments, and study the desired properties in a very controllable and clean environment. Formation of similar complex fractal flat band waveguide networks has been proposed theoretically recently [45].

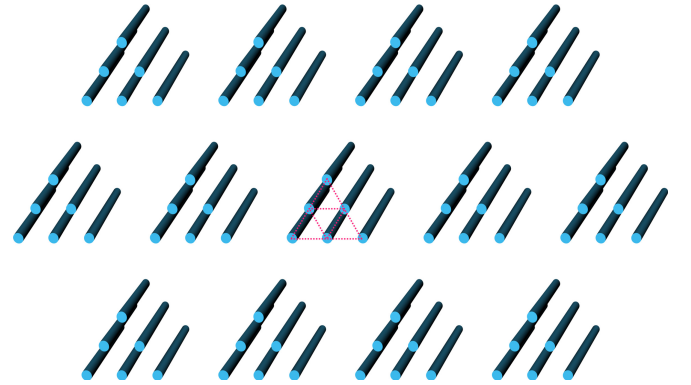


FIG. 9: Schematic diagram of a possible proposed photonic waveguide structure corresponding to the lattice structure shown in Fig. 2.

VI. CONCLUDING REMARK AND OUTLOOK

In conclusion, we have studied flat bands in a complex 2D lattice structure formed by different generations of a SPG fractal geometry as the building unit cell of the lattice. We show that such complex structure gives rise to band spectrum with notable features, such as appearance of isolated gapped FB states, or the presence of gapless single or multiple electron-like or hole-like FB states touching their nearest dispersive bands, or the formation of “Dirac-cone” with a FB state sandwiched in-between them, resembling the spin-1 conical-type energy spectrum. We furthermore show that the different combinations of staggered or non-staggered flux may tune or detune the FB states, appearing in such a complex fractal-like lattice structure. For a particular flux, we show that it is possible to separate a FB state from the other dispersive bands by a gap due to the fact that time-reversal symmetry is broken. In such situation, the FB state can be thought of as a critical point (with zero band curvature) that separates electron-like and hole-like bands with opposite band curvatures, and such transition may lead to an anomalous Hall effect [36, 37]. We also show that in some cases, FB is degenerate with one or more other bands at a single point. Such band touching is accidental and can be removed by means of some perturbations.

In addition to these interesting band features, we establish a generic formula to determine the number of FB states as a function of the fractal generation index, ℓ . Finally, we address the possibility of realizing our model in a photonic waveguide network which can be fabricated by using single mode optical waveguides in highly controllable environment using femtosecond laser pulses [22, 23].

The fractal FB model proposed by us has gone beyond the paradigm of regular flat band lattice geometries such as Lieb lattice, hexagonal lattice, Kagome lattice, etc., and can be a new prospective lattice model to explore different physical phenomena. For example, topological protection of band touching in the ma-

jority of geometrically frustrated systems are known through a careful counting of linearly independent localized states [35]. Since our proposed model exhibits both linear and quadratic band touching in a single lattice setting for a particular configuration of the parameters, topological protection in these settings may differ significantly from the typical frustrated lattice systems as discussed in Ref. [35]. Note that such study is required to understand the physics of interacting bosons and fermions in flat bands with various filling for short-range interactions of arbitrary strength.

On a related note, our proposed model with $\ell = 1$ resembles to the lattice structure of a new class of magnetic materials, namely triangular Kagome lattices. This lattice structure is formed by extra set of triangles inside the Kagome triangles. While solving Hubbard model in this “triangle-in-triangle” lattice structure, several new phases such as plaquette insulator, Kondo metal can be obtained while asymmetry is introduced in the sys-

tem [46]. In view of that, we believe our proposed model may give rise to even richer phases as a function of interaction, temperature and asymmetry. Overall, our findings provide a concrete framework for future studies, addressing the nature of many-body ground state in the presence of repulsive interactions and at fractional filling. Moreover, it may grow interests to explore the possibility of having FB states in lattice structures formed by other interesting fractal geometries such as Vicsek and Koch fractal.

Acknowledgments

BP would like to acknowledge Anne E. B. Nielsen and Arunava Chakrabarti for useful discussions on related topics. We thank the referees for constructive comments.

-
- [1] M. Goda, S. Nishino, and H. Matsuda, *Phys. Rev. Lett.* **96**, 126401 (2006).
 - [2] J. T. Chalker, T. S. Pickles, and P. Shukla, *Phys. Rev. B* **82**, 104209 (2010).
 - [3] S. Nishino, H. Matsuda, and M. Goda, *J. Phys. Soc. Jpn.* **76**, 024709 (2007).
 - [4] M. Niță, B. Ostahie, and A. Aldea, *Phys. Rev. B* **87**, 125428 (2013).
 - [5] S. Nishino, M. Goda, and K. Kusakabe, *J. Phys. Soc. Jpn.* **72** 2015 (2003).
 - [6] S. Nishino and M. Goda, *J. Phys. Soc. Jpn.* **74** 393 (2005).
 - [7] M. Hyrkäs, V. Apaja, and M. Manninen, *Phys. Rev. A* **87**, 023614 (2013).
 - [8] S. Endo, T. Oka, and H. Aoki, *Phys. Rev. B* **81**, 113104 (2010).
 - [9] D. Leykam, S. Flach, O. Bahat-Treidel, and A. S. Desyatnikov, *Phys. Rev. B* **88**, 224203 (2013).
 - [10] S. Flach, D. Leykam, J. D. Bodyfelt, P. Matthies, and A. S. Desyatnikov, *Europhys. Lett.* **105**, 30001 (2014).
 - [11] J. D. Bodyfelt, D. Leykam, C. Danieli, X. Yu, and S. Flach, *Phys. Rev. Lett.* **113**, 236403 (2014).
 - [12] C. Danieli, J. D. Bodyfelt, and S. Flach, *Phys. Rev. B* **91**, 235134 (2015).
 - [13] R. Khomeriki and S. Flach, *Phys. Rev. Lett.* **116**, 245301 (2016).
 - [14] W. Maimaiti, A. Andreanov, H. C. Park, O. Gendelman, and S. Flach, *Phys. Rev. B* **95**, 115135 (2017).
 - [15] A. Ramachandran, A. Andreanov, and S. Flach, *Phys. Rev. B* **96**, 161104(R) (2017).
 - [16] T. Kimura, H. Tamura, K. Shiraishi, and H. Takayanagi, *Phys. Rev. B* **65**, 081307(R) (2002).
 - [17] A. Tanaka and H. Ueda, *Phys. Rev. Lett.* **90**, 067204 (2003).
 - [18] F. Pollmann, P. Fulde, and K. Shtengel, *Phys. Rev. Lett.* **100**, 136404 (2008).
 - [19] K. Sun, Z. Gu, H. Katsura, and S. Das Sarma, *Phys. Rev. Lett.* **106**, 236803 (2011).
 - [20] E. Tang, J.-W. Mei, and X.-G. Wen, *Phys. Rev. Lett.* **106**, 236802 (2011).
 - [21] T. Neupert, L. Santos, C. Chamon, and C. Mudry, *Phys. Rev. Lett.* **106**, 236804 (2011).
 - [22] R. A. Vicencio, C. Cantillano, L. Morales-Inostroza, B. Real, C. Mejía-Cortés, S. Weimann, A. Szameit, and M. I. Molina, *Phys. Rev. Lett.* **114**, 245503 (2015).
 - [23] S. Mukherjee, A. Spracklen, D. Choudhury, N. Goldman, P. Öhberg, E. Andersson, and R. R. Thomson, *Phys. Rev. Lett.* **114**, 245504 (2015).
 - [24] S. Mukherjee and R. R. Thomson, *Opt. Lett.* **40**, 5443 (2015).
 - [25] S. Longhi, *Opt. Lett.* **39**, 5892 (2014).
 - [26] D. Guzmán-Silva, C. Mejía-Cortés, M. A. Bandres, M. C. Rechtsman, S. Weimann, S. Nolte, M. Segev, A. Szameit, and R. A. Vicencio, *New J. Phys.* **16**, 063061 (2014).
 - [27] S. Xia, Y. Hu., D. Song, Y. Zong, L. Tang, and Z. Chen, *Opt. Lett.* **41**, 1435 (2016).
 - [28] Y. Zong, S. Xia, L. Tang, D. Song, Y. Hu, Y. Pei, J. Su, Y. Li, and Z. Chen, *Opt. Express* **24**, 8877 (2016).
 - [29] S. Weimann, L. Morales-Inostroza, B. Real, C. Cantillano, A. Szameit, and R. A. Vicencio, *Opt. Lett.* **41**, 2414 (2016).
 - [30] V. Apaja, M. Hyrkäs, and M. Manninen, *Phys. Rev. A* **82**, 041402(R) (2010).
 - [31] I. Bloch, J. Dalibard, and W. Zwerger, *Rev. Mod. Phys.* **80**, 885 (2008).
 - [32] N. Goldman, D. F. Urban, and D. Bercioux, *Phys. Rev. A* **83**, 063601 (2011).
 - [33] N. Masumoto, N. Y. Kim, T. Byrnes, K. Kusudo, A. Löffler, S. Höfling, A. Forchel, and Y. Yamamoto, *New J. Phys.* **14**, 065002 (2012).
 - [34] S. D. Huber and E. Altman, *Phys. Rev. B* **82**, 184502 (2010).
 - [35] D. L. Bergman, C. Wu, and L. Balents, *Phys. Rev. B* **78**, 125104 (2008).
 - [36] D. Green, L. Santos, and C. Chamon, *Phys. Rev. B* **82**, 075104 (2010).
 - [37] K. Ohgushi, S. Murakami, and N. Nagaosa, *Phys. Rev. B* **62**, R6065(R) (2000).

- [38] C. Wu, D. Bergman, L. Balents, and S. Das Sarma, *Phys. Rev. Lett.* **99**, 070401 (2007).
- [39] X. R. Wang, *Phys. Rev. B* **51**, 9310 (1995); J. H. Luscumbe and R. C. Desai, *Phys. Rev. B* **32**, 1614 (1985).
- [40] E. Dagotto, E. Fradkin, and A. Moreo, *Phys. Lett. B* **172**, 383 (1986).
- [41] G. Möller and R. Moessner, *Phys. Rev. Lett.* **96**, 237202 (2006).
- [42] F. D. M. Haldane, *Phys. Rev. Lett.* **61**, 2015 (1988).
- [43] B. Pal and A. Chakrabarti, *Phys. Rev. B* **85**, 214203 (2012).
- [44] S. Longhi, *Opt. Lett.* **38**, 3570 (2013).
- [45] A. Nandy and A. Chakrabarti, *Phys. Rev. A* **93**, 013807 (2016).
- [46] Y.-H. Chen, H.-S. Tao, D.-X. Yao, and W.-M. Liu, *Phys. Rev. Lett.* **108**, 246402 (2012).